AIAA JOURNAL
Vol. 46, No. 11, November 2008

Experimental and Numerical Study of Cooling Gas Injection in Laminar Supersonic Flow

K. A. Heufer* and H. Olivier†
Rheinisch Westfälischen Technischen Hochschule Aachen University, 52056 Aachen, Germany

DOI: 10.2514/1.34218

In this study, we investigate film cooling on an inclined flat plate in a laminar supersonic flow. The influence of the most relevant parameters, the Mach and Reynolds numbers of the freestream, the blowing ratio, and the blowing geometry, is examined using numerical simulations and in experiments. Importantly, a correlation factor that describes the effect of the most important parameters for a large range of flow conditions has been developed from a simple heat balance model. Unlike the results for turbulent conditions that are typical for cooling turbine blades, interestingly, we have found that considerably less cooling gas mass flows are needed to cool the surface over a large area. In laminar boundary layers no turbulence appears, so that neither the cooling gas strongly mixes with the main stream nor does the blowing momentum influence the cooling effectiveness, provided that a boundary-layer transition is not induced by the cooling gas injection. Our results, presented here, agree with the results of previous investigations of laminar supersonic flow conditions.

Nomenclature

C^*	=	Chapman–Rubesin factor
c_p	=	specific thermal capacity
F	=	blowing ratio
$F(U)$	=	flux vector in the x direction
$G(U)$	=	flux vector in the y direction
$H(U)$	=	vector of the viscosity terms
h	=	enthalpy
k	=	thermal conductivity
M	=	momentum ratio
Ma	=	Mach number
$\dot{m}_c$	=	cooling gas mass flow
$\dot{m}'_e$	=	mass flow entering the mixing layer from the main flow
Pr	=	Prandtl number
$\dot{q}$	=	wall heat flux
Re_e	=	unit Reynolds number behind the front shock
$Re_{x'}$	=	Reynolds number based on x'
s	=	slot width in the streamwise direction
$\bar{T}$	=	mean temperature in the mixing layer
$T_{\mathrm{aw},c}$	=	adiabatic wall temperature for the case with cooling
T_r	=	recovery temperature
$T_{0,c}$	=	total temperature of the cooling gas
t	=	slot width in the spanwise direction
U	=	state vector
u	=	velocity in the x direction
v	=	velocity in the y direction
x	=	distance from the leading edge, parallel to the model surface
x_{ref}	=	empirical reference length
x_s	=	distance from the leading edge to the center of the blowing opening
x'	=	distance from the center of the blowing opening
y	=	distance normal to the model surface
δ	=	boundary-layer thickness
η	=	cooling effectiveness
λ	=	heat transfer coefficient
μ	=	dynamic viscosity
ξ	=	correlation factor
ρ	=	density
σ	=	Mach angle
Ω	=	blowing angle

Subscripts

c	=	with cooling
nc	=	no cooling
e	=	boundary-layer edge
∞	=	freestream
0	=	stagnation conditions

Superscript

*	=	values determined at the reference temperature

I. Introduction

MOST of today's thermal protection systems (TPS) for hypersonic flight vehicles can be described as passive, that is, they cannot be adjusted to the actual heat loads during flight and they do not directly affect the flow around the body to reduce the thermal loads. Therefore, the peak heat load is the design criterion for the entire flight path. An apt example of this kind of TPS is the heat shield of the American space shuttles. Here, materials with very low thermal conductivities are used to protect the main structure from heat loads during reentry into the atmosphere [1]. For different vehicle regions that show varying heat loads, the TPS is adapted such that diverse materials and wall thicknesses are used to reduce the weight of the TPS as much as possible. Mostly laminar flow conditions take place during the critical reentry phase, and the postshock Mach number typically varies from 1 to 4 at a 40 deg angle of attack. Turbulent boundaries occur only further downstream from the leading edges and near deflected flaps where shock boundary-layer interactions take place.

One alternative to passive thermal protection systems is the active film-cooling technique, which is currently state of the art for cooling turbine blades. In this technique, mostly air is applied as cooling gas is introduced into the outer flow, which establishes a cooling film along the surface to reduce the heat flux penetrating into the wall. Initial investigations concerning film cooling have been performed for quasi-two-dimensional slot-blowing configurations. However, in modern turbine blades, the cooling gas is injected through shaped holes at the surface to achieve a maximum cooling effect.

Received 23 August 2007; revision received 10 June 2008; accepted for publication 19 June 2008.

*Research Engineer, Shock Wave Laboratory, Templergraben 55.
†Professor, Shock Wave Laboratory, Templergraben 55. Member AIAA.

A comprehensive overview of previous studies concerning film cooling is given in [2]. Therein, theoretical approaches based on an energy balance in the boundary layer are presented to predict the cooling effectiveness in an incompressible, turbulent boundary-layer flow. Furthermore, results of various experimental studies are summarized and compared with theoretical models. In most of the investigations presented in [2], very low freestream Mach numbers ranging from 0.02 to 0.2 have been employed. Usually, in such investigation, air is used in the freestream and as the cooling gas. Concerning slot film cooling, numerous investigations have been performed in the past showing the relevant physical phenomena and important parameters [3–5].

Recent works concerning the cooling of turbine blades mostly deal with single-hole injection and the resulting interaction of the freestream and the cooling gas jets [6–10]. In this case, the flowfield is dominated by three-dimensional vorticity structures. Usually, these vortices reduce the average cooling effectiveness. Many investigations have been conducted to reduce the intensity of these vortices, for example, by lowering the blowing angle or by shaping the blowing opening at the surface [7–9] These studies have been performed for turbulent, subsonic flow conditions that are typical for turbine flows.

However, for supersonic flow conditions and turbulent boundary layers, film cooling has been investigated by employing tangential slot injection [11–14]. One possible application of this is the cooling of scramjet combustion chambers. In these experiments, the ratio of the specific cooling gas mass flow to the corresponding specific freestream mass flow was less than the ratio for turbine blade cooling. In [11], a correlation factor has been found based on Goldstein's approach [2] to correlate the results for different blowing parameters.

Supersonic tangential injection has also been investigated for laminar flow conditions [15]. Here, different cooling gases have been injected along a flat plate behind a downstream-facing step. Compared with turbulent flow conditions, a significantly higher cooling effectiveness is achieved for similar cooling gas mass flows.

Nontangential gas injection is used for fuel injection in scramjets [16]. In these scramjets, the fuel is injected using different injection angles. In this case, the fuel gas deeply penetrates into the main stream due to high blowing momentum, which results in a strong mixing of the injected gas with the freestream and the formation of a bow shock in front of the blowing opening. Regarding a desired cooling of the surface, these effects have to be avoided; therefore, much lower blowing ratios than for fuel injection are necessary.

Another application field for active cooling is the so-called transpiration cooling, in which the cooling gas is not injected through single holes but through porous walls. Besides the film-cooling effect, an additional cooling effect in the wall can be achieved. Theoretical and experimental studies concerning transpiration cooling were published as early as the 1960s [15,16]. In newer concepts, the active cooling technique is used to cool rocket combustion chambers, wherein hydrogen is injected through porous walls into the combustion chamber [17,18].

All these studies show that the active cooling technique is an effective method for lowering structural thermal loads. This has motivated us to prove the feasibility of this technique to cool reentry vehicles during the critical phase of maximum heat loading. Contrary to the aforementioned investigations, this work deals with the film-cooling technique as applied to laminar flows using low injection rates, nontangential injection, and supersonic flow conditions at the boundary-layer edge as they occur behind the front shock of hypersonic flight vehicles.

Besides the capacity for thermal protection, another aspect of a TPS is its reliability. Previously, it became obvious that a small local failure of the TPS can cause a catastrophic failure of the flight vehicle. A suitable active cooling system increases the reliability of the TPS, because a local failure of the system can be compensated for with sufficient cooling capacity upstream from the damaged part. The aim of this paper is to experimentally and numerically examine the fundamental flow phenomena and the performance of active cooling in hypersonic flows. This cooling technique may additionally reduce the structural weight of the flight vehicle with its high effectiveness.

II. General Description of the Flow Problem

To fundamentally investigate film cooling in hypersonic flows, an inclined flat plate is chosen as the reference case. Furthermore, experiments are performed at low enthalpy conditions to avoid any real gas effects, that is, ideal gas behavior can be assumed. Because flow parameters for this case without cooling have been examined intensively in previous analytical, numerical, and experimental studies [19,20], reliable reference data for the inviscid as well as the viscous flow are available. In our study, the flow problem can be regarded as two dimensional, because the blowing slots have a sufficient span.

Ideally, by injecting a cooling gas, a film forms over the surface and separates the hot flow from the wall. As a result of this added mass in the boundary layer, it becomes thicker, leading to lower velocity and temperature gradients at the wall. Moreover, both the viscosity and the thermal conductivity are reduced by the lower cooling gas temperature. This causes lower heat fluxes and friction forces at the wall. In addition, this effect can be influenced by the heat capacity of the cooling gas. Furthermore, the different flow conditions between the injected cooling gas and the hot main flow result in gradients between these two layers (Fig. 1). With an increasing distance from the blowing opening, these gradients become smaller and the boundary-layer profiles approach the undisturbed ones so that the temperature and velocity gradients at the wall increase again. Moreover, a mixing between the two gases can be expected, which reduces the cooling effect further downstream from the blowing opening. In contrast to this, an increasing cooling effect is expected with an increasing cooling gas mass flow.

One of the main parameters of the cooling process is the blowing ratio, F, defined as the specific mass flow ratio of the cooling gas and the freestream at the boundary-layer edge:

$$F = \frac{\rho_c u_c}{\rho_e u_e} \tag{1}$$

Furthermore, the momentum ratio, M, between the cooling gas and the main flow has been found as an important parameter for film cooling in turbulent flows:

$$M = \frac{\rho_c u_c^2}{\rho_e u_e^2} = F^2 \frac{\rho_e}{\rho_c} \tag{2}$$

To describe an active cooling system, a cooling effectiveness, η, is defined. The following definition for a stationary flow is common in the literature concerning the cooling of turbine blades:

$$\eta = \frac{T_r - T_{\mathrm{aw},c}}{T_r - T_{0,c}} \tag{3}$$

where T_r indicates the recovery temperature of the flow, $T_{\mathrm{aw},c}$ the adiabatic wall temperature for the case with cooling, and $T_{0,c}$ the reservoir temperature of the cooling gas.

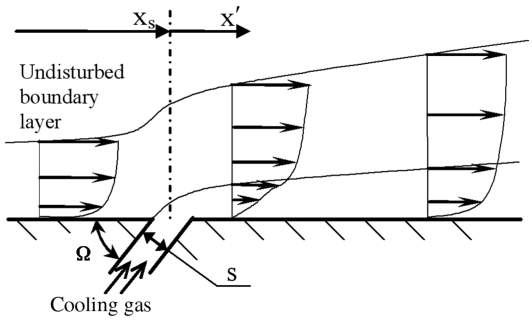

Fig. 1 Principle of film cooling.

For impulse test facilities, especially for shock tunnels as used in this study for performing experiments, a transformation of the adiabatic temperatures to the measurable wall heat fluxes is necessary, because the adiabatic wall temperature is not reached during the short testing time. This transformation is similar to the approach given in [11]. In general, the heat flux to the surface can be expressed as follows:

$$\dot{q} = \lambda \cdot (T_{\mathrm{aw}} - T_w) \tag{4}$$

The maximum change of the surface temperature of the heat flux sensor during the experiments is about 2 K for the investigated flow conditions. Regarding the recovery temperature, this temperature change is negligible for determining the heat flux to the wall. Thus, the wall temperature can be assumed to be constant at room temperature. By applying Eq. (4) to the case with cooling (c) and the case without cooling (nc), we obtain an expression for the adiabatic wall temperature in the case with cooling:

$$T_{\mathrm{aw},c} = T_{\mathrm{aw,nc}} - \frac{\dot{q}_{\mathrm{nc}}}{\lambda_{\mathrm{nc}}} + \frac{\dot{q}_c}{\lambda_c} \tag{5}$$

For the case without cooling, the adiabatic wall temperature is equal to the recovery temperature of the freestream. Moreover, the reservoir temperature of the cooling gas is also equal to the ambient temperature for the considered cases. This leads to a simple formula of the cooling effectiveness by inserting Eq. (5) into Eq. (3):

$$\eta = 1 - \frac{\dot{q}_c}{\dot{q}_{\mathrm{nc}}} \tag{6}$$

For experiments with the same gas used as coolant and in the main flow, the heat transfer coefficients λ_c and λ_{nc} are assumed to be equivalent. The temperature level in the region near the wall for both cases is close to the wall temperature for the considered case of isothermal walls, and the cooling gas reservoir temperature is equal to the wall temperature. This leads to constant heat transfer coefficients, provided that the flow is not disturbed significantly by injecting the cooling gas, that is, the thickness of the cooling gas layer is small compared with the thickness of the undisturbed boundary layer (Fig. 1). The validity of this assumption has already been shown in previous experimental studies for low blowing ratios [2]. A measurable change of the heat transfer coefficient has been reported only close to the injection position in combination with high blowing ratios ($F > 0.5$). Thus, the assumption of $\lambda_c = \lambda_{\mathrm{nc}}$ is valid for the low blowing ratios of the present study ($F = 0$–0.15). This is also proved in Sec. VI.E, in which numerical results for the cases of isothermal and adiabatic wall conditions are compared. If, for high blowing ratios and high blowing momentum, the cooling gas layer cannot be regarded as a thin layer or the oncoming boundary layer is significantly disturbed by the cooling gas injection, the presented assumption is no longer valid.

III. Theoretical Approach

A theoretical approach for predicting the cooling effectiveness based on the approach of [2] is presented. In a first step, the influence of the injection to the oncoming boundary layer is neglected, and a low speed flow ($Ma_e \ll 1$) is assumed. Furthermore, it is presumed that the injected cooling gas and the gas of the main flow form a mixing layer starting at the slot position (Fig. 2).

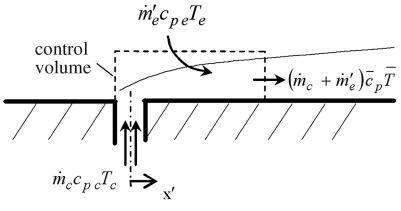

Fig. 2 Control volume for energy balance.

Moreover, a well-mixed flow in the mixing layer, constant ideal gas properties, and adiabatic walls are assumed. In this case, the following energy balance holds, wherein the work performed by viscous forces and variations of the kinetic energy have been neglected:

$$(\dot{m}_c + \dot{m}'_e)\bar{c}_p \bar{T} = \dot{m}_c c_{pc} T_c + \dot{m}'_e c_{pe} T_e \tag{7}$$

The average specific heat is given by the following expression:

$$\bar{c}_p = \frac{\dot{m}_c c_{pc} + \dot{m}'_e c_{pe}}{\dot{m}_c + \dot{m}'_e} \tag{8}$$

For $Ma_e \ll 1$, the recovery temperature of the flow is approximately equal to the temperature at the boundary-layer edge ($T_r \approx T_e$). Furthermore, we assume that the mean temperature $\bar{T}$ is constant along the mixing layer height and is equal to the adiabatic wall temperature in the case of cooling ($\bar{T} = T_{\mathrm{aw},c}$). Thus, a first expression for the cooling effectiveness [Eq. (3)] is achieved:

$$\eta = \frac{T_e - \bar{T}}{T_e - T_{0,c}} = \frac{1}{1 + \frac{\dot{m}'_e c_{pe}}{\dot{m}_c c_{pc}}} \tag{9}$$

In [2], the mass flow $\dot{m}'_e$, which enters the mixing layer from the main flow, is assumed to be equal to the mass flow of a fictitious undisturbed boundary layer starting from the injection position ($x' = 0$). To determine this mass flow, a simplified approach of the third order is assumed for the velocity profile in the boundary layer as follows:

$$u/u_e = a + b(y/\delta) + c(y/\delta)^2 + d(y/\delta)^3 \tag{10}$$

The usual boundary conditions for the velocity profile lead to

$$u/u_e = \tfrac{3}{2}(y/\delta) - \tfrac{1}{2}(y/\delta)^3 \tag{11}$$

which approximates the Blasius solution.

Finally, this yields an expression for the mass flow $\dot{m}'_e$:

$$\dot{m}'_e = \int_0^{\delta'} \rho_e u_e \left(\frac{3}{2}(y/\delta) - \frac{1}{2}(y/\delta)^3\right) \mathrm{d}y = \frac{5}{8}\rho_e u_e \delta' \tag{12}$$

The boundary-layer thickness in a laminar incompressible flow over a flat plate is given by Eq. (13):

$$\delta' \approx 4.64 \cdot x' \cdot Re_{x'}^{-0.5} \tag{13}$$

The cooling gas mass flow can be determined by the following expression:

$$\dot{m}_c = \rho_c u_c s = F s\, \rho_e u_e \tag{14}$$

Inserting Eqs. (12) and (14) into Eq. (9) leads to the following equation for the cooling effectiveness in laminar, incompressible boundary-layer flows:

$$\eta = \frac{1}{1 + 2.9 \frac{c_{pe}}{c_{pc}} \frac{\sqrt{x'/s}}{F} \left(\frac{\rho_e u_e s}{\mu_e}\right)^{-0.5}} \tag{15}$$

This expression for the cooling effectiveness has been derived under some rough assumptions. Unlike the assumption of a constant temperature in the mixing layer, in reality, there is a temperature profile in the mixing layer and so the adiabatic wall temperature will be lower than the mean temperature of the mixing layer. This results in a higher cooling effectiveness. Furthermore, the influence of the oncoming boundary layer has been neglected, which is important for the interaction between the cooling gas and the main flow. Nevertheless, the experimental investigations of turbulent flows basically show good agreement with this simple approach [2]. In the following [Eqs. (16–18)], a correlation factor will be developed based on Eq. (15). Starting from a known solution, in which all physical effects are captured, this correlation factor describes the effect of changing flow conditions. Finally, this results in one curve

for the cooling effectiveness as a function of the correlation factor, which is independent of the freestream parameters and the blowing parameters. This approach is true provided that similar flowfields are considered.

According to Eq. (15), the cooling effectiveness shows the following dependency for the same gases as the cooling gas and in the main flow:

$$\eta = f\left(\frac{\sqrt{x'}}{Fs}\cdot\frac{1}{\sqrt{Re_e}}\right) \tag{16}$$

Two effects have to be considered to extend this dependency to the influence of the oncoming boundary layer and its thickening resulting from the cooling gas injection. First, the boundary layer is initially thickened at the slot position and this thickening decreases relative to the undisturbed boundary layer with the regular boundary-layer growth, which is proportional to $x^{0.5}$. Second, the gradients within the boundary layer decrease with increasing distance from the leading edge to the slot position, x_s, which leads to a weaker heating of the cooling gas and, thus, a higher cooling effectiveness. This effect has been covered by an empirically determined reference length, $x_{\text{ref}} = (x_s)^{1.16}$, with x_{ref} and x_s in meters. In the strict sense, this reference length only holds for the considered geometry and the considered range of the slot position, x_s, ranging from 0.055 up to 0.565 m. Finally, these two effects result in an additional parameter, $(x/x_{\text{ref}})^{0.5}$.

Moreover, the reference enthalpy method is applied to include compressibility effects [2]. Here, the temperature dependent parameters, that is, the density and the viscosity, are evaluated at the reference temperature T^*:

$$T^* = 0.28T_e + 0.72T_r \tag{17}$$

By applying this method to the correlation [Eq. (16)], we obtain an additional term: $(\rho^*\mu^*)^{0.5}(\rho_e\mu_e)^{-0.5}$. This factor is equal to the square root of the Chapman–Rubesin factor, C^*, which describes the thermal viscosity effects in compressible boundary layers [21]. Similar to the Reynolds, Mach, and Prandtl numbers, the Chapman–Rubesin factor is a relevant similitude parameter for supersonic boundary layers without a pressure gradient. Finally, we obtain the following definition of the correlation factor:

$$\xi = \frac{\sqrt{x'}}{Fs}\frac{1}{\sqrt{Re_e}}\sqrt{\frac{x}{x_{\text{ref}}}}\sqrt{C^*} \tag{18}$$

which is used to correlate experimental and numerical data for a variety of conditions in Sec. VI.

It is worth noting that another simple physical model of the film cooling also leads to the same correlation factor given in Eq. (18). This model is based on estimating the energy transport into the cooling gas layer as a heat flux from the main flow. Thereby, the heat flux into the cooling gas layer is determined by assuming this heat flux to be equal to the heat flux of an undisturbed laminar boundary layer starting from the slot position. The reference wall temperature for determining this heat flux is set as the local cooling gas temperature. Contrary to the model described earlier, this heat conduction model does not consider a mixing process between the cooling gas and the main flow.

IV. Experimental Setup

A. Model

A wedge-shaped setup is used for the experimental model (Fig. 3). The test surface has a 30 deg angle of attack to the freestream for this reference configuration. The model is equipped with up to 30 coaxial thermocouples and 20 pressure gauges to determine the heat flux and pressure distribution, respectively [22]. Moreover, black polyvinyl chloride with a high emission factor was chosen as a surface material to allow infrared measurements. An infrared camera was used to achieve a qualitative overview of the temperature distribution on the surface. The inclined plate has a width of 350 mm and a length of

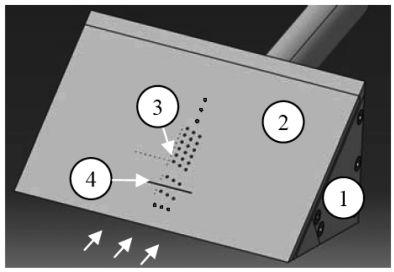

Fig. 3 Model with sharp leading edge: 1) support structure, 2) test plate, 3) probe positions, and 4) blowing slot.

250 mm in the streamwise direction. In general, the slot length in spanwise direction is 120 mm. Slots of shorter length have been used to investigate the influence of a finite slot length. The different slot configurations investigated experimentally and numerically and the corresponding results are described in Sec. VI. The notation of the geometrical parameters is given in Fig. 1.

B. Test Facility

For the experiments, the shock tunnel TH2 of the Shock Wave Laboratory is employed. The shock tunnel can be operated in the helium-driven mode or with a detonation driver [23,24]. Low enthalpy conditions that ensure perfect gas behavior are employed for the experiments. The corresponding freestream values are listed in Table 1. To determine the blowing ratio and the correlation factor, respectively, the flow conditions at the boundary-layer edge have to be known. To achieve these values, the flow conditions behind the front shock of the model are determined by assuming ideal gas behavior. This is justified by the relatively low total temperatures of the test flow. These values behind the shock are listed in Table 1 for a deflection angle of 30 deg and are used as the freestream conditions on a flat plate for the numerical simulation. Previous experimental studies have shown constant freestream conditions and a constant blowing ratio during the measuring time of about 2 ms [25].

V. Numerical Method

A. General Description

For the numerical simulation, a computational fluid dynamics (CFD) code has been developed to solve the two-dimensional compressible Navier–Stokes equations for ideal gases. The solution method uses a Cartesian grid with nonequidistant grid cells. In general, the calculation is divided into two parts. First, the Navier–Stokes equations are simplified by neglecting the viscosity terms. This leads to the Euler equations presented in the conservative form in Eq. (19):

$$\frac{\partial U}{\partial t}+\frac{\partial F(U)}{\partial x}+\frac{\partial G(U)}{\partial y}=0$$

$$U=\begin{pmatrix}\rho\\ \rho u\\ \rho v\\ E\end{pmatrix},\quad F(U)=\begin{pmatrix}\rho u\\ \rho u^2+p\\ \rho uv\\ u(E+p)\end{pmatrix},\quad G(U)=\begin{pmatrix}\rho v\\ \rho uv\\ \rho v^2+p\\ v(E+p)\end{pmatrix} \tag{19}$$

These homogeneous partial differential equations are solved by assuming constant parameters in the grid cells. By using an exact Riemann solver, the fluxes at the cell interfaces are determined by the weighted average flux method (WAF) [26]. These fluxes and the values of the former time step, n, allow the determination of the solution vector of the new time step, $n+1$, by employing an explicit formulation of the following form:

$$U_{i,J}^{n+1} = U_{i,j}^{n} + (\Delta t/\Delta x)(F_{i-\frac{1}{2},j} - F_{i+\frac{1}{2},j}) + (\Delta t/\Delta y)(G_{i,j-\frac{1}{2}} - G_{i,j+\frac{1}{2}}) \tag{20}$$

Table 1 Flow conditions

	Condition Ia		Condition Ib	
	Freestream (∞)	Behind front shock (e)	Freestream (∞)	Behind front shock (e)
T_0, K	1110	1110	1420	1420
u, m/s	1470	1150	1690	1310
p, Pa	435	13,740	375	12,540
T, K	80	488	96	620
T_w, K	——	293	——	293
Re, 10^6/m	5.3	4.3	3.58	3.0
Ma	8.3	2.6	8.4	2.6

The WAF scheme is second-order accurate in space and time, whereby oscillations of the solution in regions of high gradients are limited with van Albada's method. The time step, Δt, is determined by the Courant–Friedrichs–Lewy (CFL) condition. After the Euler equations are solved, the viscous terms are taken into account in a second step by solving the ordinary differential equations of the following form:

$$\frac{\mathrm{d}U}{\mathrm{d}t} = H(U) \tag{21}$$

with

$$H(U) = \begin{pmatrix} 0 \\ \frac{\partial}{\partial x}(R_1) + \frac{\partial}{\partial y}(R_2) \\ \frac{\partial}{\partial x}(R_3) + \frac{\partial}{\partial y}(R_4) \\ \frac{\partial}{\partial x}(R_5) + \frac{\partial}{\partial y}(R_6) \end{pmatrix}$$

$$R_1 = \eta\left(\frac{4}{3}\frac{\partial u}{\partial x} - \frac{2}{3}\frac{\partial v}{\partial y}\right), \qquad R_2 = \eta\left(\frac{\partial u}{\partial y} + \frac{\partial v}{\partial x}\right)$$

$$R_3 = \eta\left(\frac{\partial u}{\partial y} + \frac{\partial v}{\partial x}\right), \qquad R_4 = \eta\left(\frac{4}{3}\frac{\partial v}{\partial y} - \frac{2}{3}\frac{\partial u}{\partial x}\right)$$

$$R_5 = u\eta\left(\frac{4}{3}\frac{\partial u}{\partial x} - \frac{2}{3}\frac{\partial v}{\partial y}\right) + v\eta\left(\frac{\partial u}{\partial y} + \frac{\partial v}{\partial x}\right) + k\frac{\partial T}{\partial x}$$

$$R_6 = u\eta\left(\frac{\partial u}{\partial y} + \frac{\partial v}{\partial x}\right) + v\eta\left(\frac{4}{3}\frac{\partial v}{\partial y} - \frac{2}{3}\frac{\partial u}{\partial x}\right) + k\frac{\partial T}{\partial y}$$

Thereby, the ordinary differential equation is solved by using a two-step Runge–Kutta scheme. The velocity and temperature gradients on the right-hand side of Eq. (21) are determined applying a central difference scheme. The viscosity, η, is given by Sutherland's law, which is valid for perfect gas behavior. According to [19], the deviation between the viscosity given by the Sutherland's law and the viscosity resulting from an equilibrium air model is negligible for temperatures of up to 2500 K. Chemical effects such as dissociation and recombination can still be neglected for the considered temperatures of up to 2080 K. The thermal conductivity, k, is determined by assuming a constant Prandtl number. For air, the Prandtl number is set at $Pr = 0.72$.

B. Boundary Conditions and Grid

To reduce the numerical complexity as much as possible, the simple case of a flow over a flat plate is considered. The inflow conditions are set at the values behind the front shock at the leading edge of the ramp, as listed in Table 1. The flow conditions at the wall in the numerical calculation are so defined as is typical for a flat plate with no slip-wall condition, that is, the velocities are equal to zero and the pressure is equal to the pressure in the cell next to the wall. Furthermore, the temperature can be set at a fixed value for an isothermal wall condition. Otherwise, the adiabatic wall condition is applied. The outflow parameters are determined for zero-gradient boundary conditions.

For the numerical simulations, the computational domain has been divided into three parts (Fig. 4). In all parts, rectangular cells are used. The region nearest to the wall (I) features a cell height of $\Delta y = 6.25 \cdot 10^{-6}$ m and an aspect ratio of $\Delta x/\Delta y = 8$, which captures the interaction between the oncoming boundary layer and the cooling gas. The second area (II) covers the outer part of the boundary layer where the cell size is doubled and the aspect ratio regarding region I is constant. The upper part of the computational domain (III) covers the region of small gradients, so that a coarser resolution with a cell height of $\Delta y = 2.5 \cdot 10^{-5}$ m and an aspect ratio of 8 is sufficient in this region. To prove the grid resolution, the flowfield has been simulated with a halved cell size and a halved aspect ratio in all regions (I–III). Concerning the cooling effectiveness, the different grid resolutions deliver the same results so that the computations presented in Sec. VI are performed for the coarser grid (Fig. 5).

The blowing opening is simulated in two ways. First, as a simple approximation, the blowing opening is considered as a boundary condition (BC) under the assumption of a constant cooling gas temperature and constant blowing ratio along the slot. Moreover, the pressure at the blowing slot is assumed to be equal to the pressure in the flowfield so that the density and the velocity of the cooling gas at the slot position can be determined. Second, the flow in the injection slot has been simulated as part of the whole flowfield (complete slot, or CS). For the low blowing ratios considered here, a separation occurs in the injection slot just below the slot opening. This leads to a somewhat different flow topology. However, by comparing the cooling effectiveness for the cases with and without detailed numerical simulation of the flow in the injection slot, it becomes obvious that the detailed numerical slot simulation does not measurably affect the cooling effectiveness downstream of the slot (Fig. 5). For this reason, the slot has been simulated as a boundary condition (BC) in the computations presented in Sec. VI.

VI. Experimental and Numerical Results

The aim of the present study is to investigate the influence of the cooling gas injection on the flowfield in laminar supersonic flows. To characterize the influence of the important parameters, these parameters have been successively varied in a wide range. The

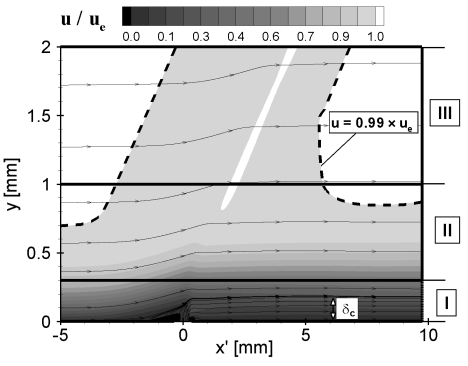

Fig. 4 Partitioning of the computational domain into three regions.

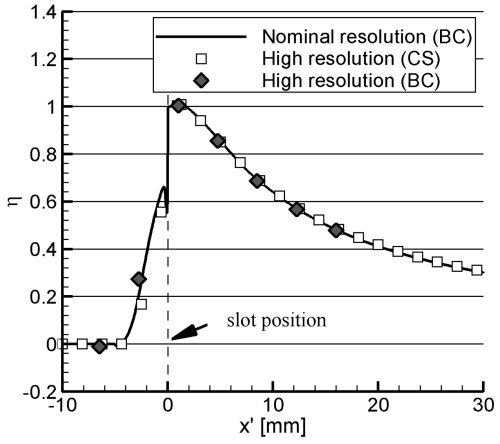

Fig. 5 Validation of the grid resolution and injection modeling for condition Ib (see Table 1).

results of these investigations are presented in the following subsections.

A. Results for the Case Without Cooling

As mentioned, the flat plate without cooling serves as the reference case to validate the numerical method and to determine the reference heat flux needed in Eq. (6). Figure 6 shows a comparison of experimental heat flux values determined from thermocouple data with a formula valid for a laminar boundary layer [19]. The heat fluxes derived from the thermocouple measurements vary between $\pm 10\%$ of the average value. This scattering of the heat flux data is caused by the relatively low heat flux values downstream of the leading edge. According to Eq. (6), a different uncertainty is expected for the cooling effectiveness. Specifically, uncertainties in the sensitivity and in the material properties of the single sensors are canceled out because of two reasons. First, the cooling effectiveness is determined by the ratio of the heat fluxes with and without cooling, that is, with the same thermocouples. Second, the heat flux is directly proportional to the material properties and the sensitivity, so that these values drop out in Eq. (6). Furthermore, the uncertainty in the cooling effectiveness behaves inversely to the cooling effectiveness itself. According to Eq. (6), the standard measurement uncertainty in the cooling effectiveness for a variation of the measured heat fluxes of $\pm 10\%$ amounts to $\Delta\eta = (1-\eta)(\pm 0.1)(2)^{0.5}$, that is, for high cooling effectiveness the uncertainty in the determined effectiveness is low. In contrast, higher uncertainties in the heat flux measurements for low heat flux levels and, as a result, for high cooling effectiveness might appear due to inferior signal-to-noise ratios. According to the previous formula, the largest error for the cooling effectiveness occurs for $\eta = 0$ and is $\Delta\eta = \pm 0.14$. This behavior of higher uncertainties with lower cooling effectiveness becomes obvious through the increasing scattering of the experimental data with decreasing cooling effectiveness (seen later in Figs. 15 and 16).

Furthermore, the velocity and temperature profiles from the numerical simulation can be compared with the solution given by van Driest for a laminar boundary layer on a flat plate [20]. Figure 7 presents a comparison of the simulation and the van Driest solution at distances from the leading edge of $x = 50$ and 90 mm. Good agreement is obtained for the velocity and temperature profiles for both positions.

B. Influence of the Cooling Gas Injection on the Flowfield

The main principle of the film-cooling process as shown in Fig. 1 is to add mass to the boundary layer by injecting the cooling gas. This leads to a thickening of the boundary layer, which causes a deflection of the main flow. The flowfield found from the numerical simulation presented in Fig. 8 for a blowing ratio of $F = 0.13$ shows exactly these effects. The main flow deflects at about 4 mm in front of the blowing opening, and the boundary-layer thickness increases as expected. In front of the blowing opening, a separation bubble is

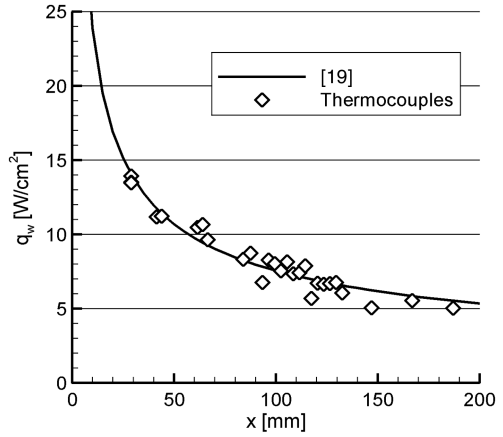

Fig. 6 Wall heat flux distribution along the flat plate for the case without cooling, condition Ib.

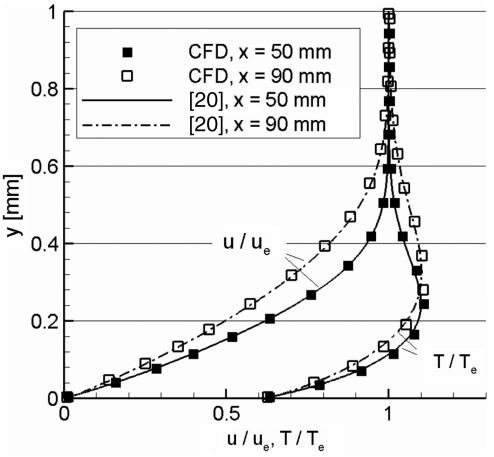

Fig. 7 Comparison of the numerical simulation and the solution given by van Driest, $F = 0$, condition Ib.

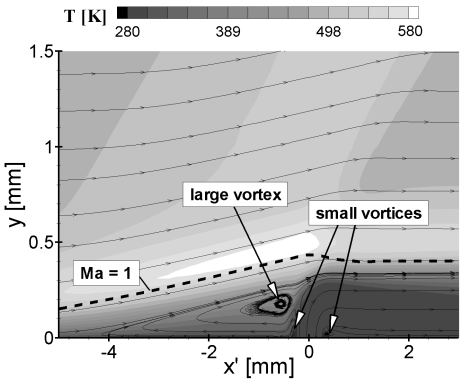

Fig. 8 Influence of the cooling gas injection on the flowfield, condition Ib, CFD.

formed by a large vortex in the subsonic part of the boundary layer. In addition, two small vortices are visible at the edges of the blowing opening. These vortices are relatively small because of the low injection velocity.

Moreover, the injection of the cooling gas strongly affects the velocity and temperature profiles downstream of the injection. Right next to the blowing opening, the wall temperature and velocity gradients are reduced to nearly zero. Further downstream from the opening, these gradients increase again until the profiles show the values of an undisturbed laminar boundary layer. This becomes apparent in Figs. 9 and 10, in which the Levy–Lees coordinate transformation is applied to compare the velocity and temperature profiles at various positions downstream from the slot.

Furthermore, the injection of the cooling gas has an effect on the outer flow. Ideally, the disturbances caused by the injection of the

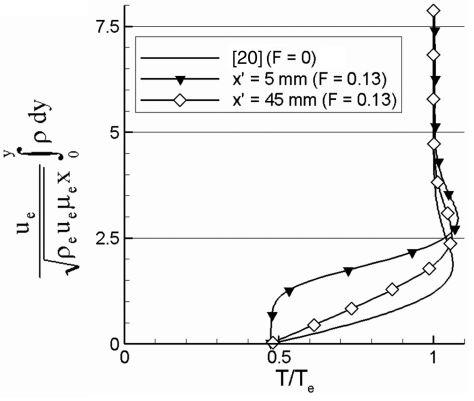

Fig. 9 Temperature profiles, condition Ia (see Table 1), CFD.

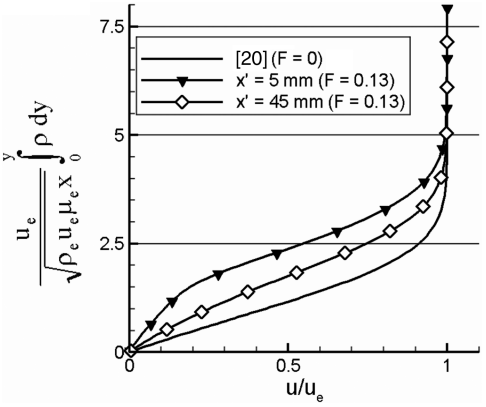

Fig. 10 Velocity profiles, condition Ia, CFD.

cooling gas should be small to achieve an optimum cooling effectiveness. A comparison of the pressure distribution and schlieren photographs for the cases with and without cooling shows the intensity of the induced disturbances. With regard to a strong blowing ratio, the injection would cause a bow shock in front of the blowing opening [27], which would lead to a higher static pressure and higher thermal loads behind this shock.

Pressure measurements presented in a previous work show no dependency of the pressure distribution on the cooling gas injection [25]. The schlieren photographs confirm the results of the pressure measurement. The deflection of the outer flow upstream of the blowing opening causes a compression wave, whereas the pressure drop behind the slot induces an expansion wave. By assuming weak disturbances, the angle of these waves with respect to the surface can be determined by the Mach angle:

$$\sin\sigma = 1/Ma_e \tag{22}$$

Knowing the Mach number behind the front shock listed in Table 1, this results in a wave angle of 22.7 deg. Figure 11 shows a schlieren photograph for a blowing ratio of $F = 0.096$. From this, a wave angle of approximately 23 deg is measured, which validates the assumption of a weak pressure wave initiated by the cooling gas injection.

The main aim of the experiments is to demonstrate the feasibility of film cooling in supersonic flows and to investigate its potential in heat reduction. Figure 12 exemplarily shows the experimentally and numerically obtained heat flux distribution along the flat plate for the case with cooling compared with the heat flux distribution for the case without cooling. Depending on the blowing ratio, the heat flux decreases a short distance upstream of the blowing opening due to the injection-induced separation and it reaches its minimum at the slot position. Further downstream from the blowing opening, the heat fluxes increase until they reach the values of the heat flux distribution for the case without cooling. According to Eq. (6), the cooling effectiveness behaves inversely to the heat flux distribution shown in Fig. 12.

C. Influence of the Blowing Ratio

To interpret the experimental results correctly, the flow behavior in the test section before the actual measuring time has to be known.

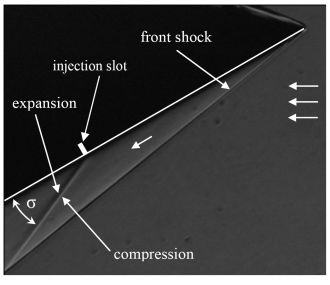

Fig. 11 Schlieren visualization of injection-induced disturbance.

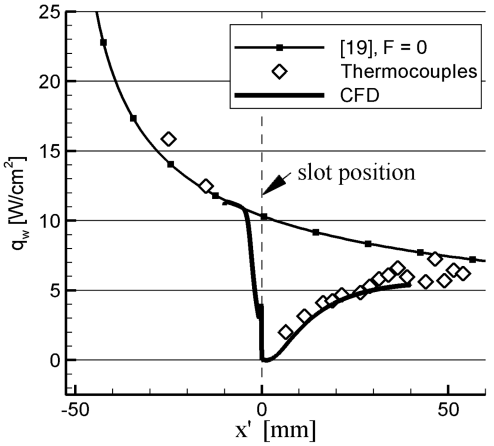

Fig. 12 Typical heat flux distribution in the case of cooling, $F = 0.096$, condition Ib.

First of all, it is not possible to switch on the cooling gas mass flow during the experiment because of the short test times in a shock tunnel. Secondly, the experimental setup requires an almost evacuated test section. That means that, before the experiment, the cooling gas is injected into the evacuated test section. This leads to a certain settling pressure in the so-called blowing chamber, which is directly installed underneath the blowing slot. While the flow establishes itself, the freestream static pressure increases, which, in turn, leads to an increasing pressure in the blowing chamber. For very low cooling gas mass flows, the pressure increase in the blowing chamber is not fast enough to establish a constant cooling gas mass flow during the measuring time. The equivalent blowing ratio is defined as the minimum blowing ratio, $F_{\min}$. An upper limit for the blowing ratio is also defined. Strong disturbances resulting from high blowing ratios may cause the transition from a laminar to a turbulent boundary layer. In this case, the wall heat flux downstream of the injection increases rapidly and the cooling effectiveness becomes negative, that is, the wall is heated up more than for the case of the laminar flow without cooling. For these blowing ratios larger than the critical blowing ratio, F_{crit}, the infrared camera detects a hot area behind the slot that indicates the boundary-layer transition (Fig. 13). A critical blowing ratio of $F_{\text{crit}} = 0.144$ has been determined for a slot width of $s = 0.5$ mm and a blowing angle of $\Omega = 90$ deg, which, according to Eq. (23), corresponds to a critical momentum ratio of $M_{\text{crit}} = 0.013$.

Presumably, the blowing momentum perpendicular to the wall is the characteristic parameter for quantifying the range of the blowing-induced boundary-layer transition, which is directly linked to the blowing ratio for fixed flow and cooling gas conditions. For all the following results, the normal blowing momentum is less than the critical one so that the flow can be regarded as fully laminar.

Within these experimental limits of $F_{\min} = 0.02$ and $F_{\text{crit}} = 0.144$, the cooling effectiveness increases with an increasing blowing ratio and it decreases with an increasing distance from the blowing opening (Fig. 14). At low blowing ratios, the dependency of the cooling effectiveness on the blowing ratio is approximately linear and asymptotically approaches the value of 1 at higher blowing ratios. The numerical results (CFD) are confirmed by the experiments shown in Fig. 15, in which the cooling effectiveness is plotted vs the correlation factor given in Eq. (18). Obviously, the

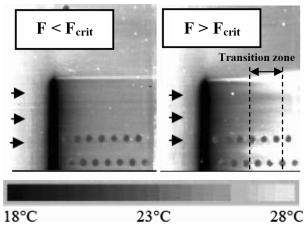

Fig. 13 Boundary-layer transition due to high blowing ratios.

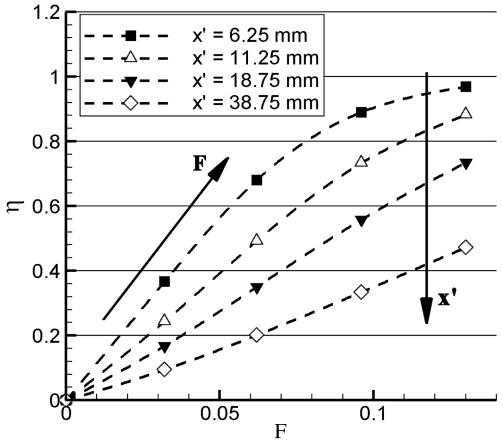

Fig. 14 Influence of the blowing ratio F, $s = 0.5$ mm, condition Ib, CFD.

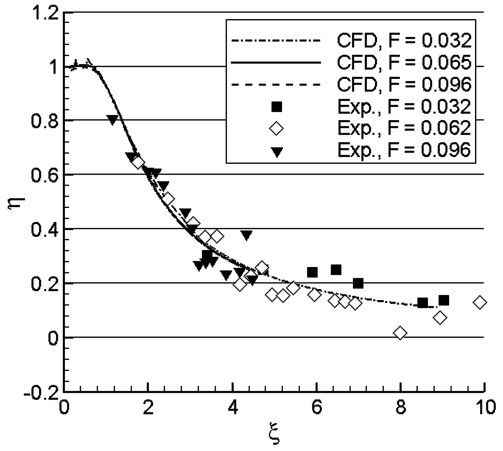

Fig. 15 Comparison of CFD and experiment for different blowing ratios, $s = 0.5$ mm, condition Ib.

different results shown in Fig. 15 are well correlated with this factor. In the literature concerning cooling turbine blades, the cooling effectiveness is typically presented as a function of the nondimensional running length, x'/s, for a given blowing ratio. Equation (18) can also be rewritten as

$$\xi = \frac{\sqrt{x'/s}}{F}\frac{1}{\sqrt{Re_s}}\sqrt{\frac{x}{x_{\text{ref}}}}\sqrt{C^*} \tag{23}$$

According to Eq. (23), the parameter x'/s is not the only scaling parameter for the cooling effectiveness. For incompressible and compressible flows, the Reynolds number with the slot width as reference length Re_s has to be taken into account. Additionally, for compressible flows, the correlation factor and, as a result, the cooling effectiveness also depend on the Chapman–Rubesin factor.

D. Influence of the Momentum Ratio

Concerning the cooling of turbine blades, the blowing geometry substantially affects the cooling effectiveness. In this case, the turbulence level in the turbulent boundary layer is influenced by the momentum ratio, M [Eq. (2)]. Low momentum ratios perpendicular to the wall cause small disturbances in the oncoming boundary layer and thus cause a weaker increase of the turbulence level due to the cooling gas injection. Finally, a low turbulence level leads to high effectiveness, because the cooling gas mixes less with the main flow. For this reason, many investigations concerning the cooling of turbine blades [7–9] have been performed to optimize the film cooling by lowering the blowing angle and shaping the exit geometry of the blowing opening. In laminar flow, however, no turbulent mixing appears and a low momentum ratio, supposedly, does not significantly influence the cooling effectiveness. Moreover, the blowing ratios and momentum ratios applied in this work are much lower than for the case of cooling turbine blades. By neglecting the influence of the cooling gas injection on the pressure distribution, the momentum ratio can be approximated by the blowing ratio and the ratio between the cooling gas temperature and the gas temperature at the boundary-layer edge:

$$M = \frac{\rho_c u_c^2}{\rho_e u_e^2} = F\frac{u_c}{u_e} = F^2\frac{\rho_e}{\rho_c} \approx F^2\frac{T_c}{T_e} \tag{24}$$

According to Eq. (24), with the experimental value $F_{\text{crit}} = 0.144$, the critical momentum triggering transition is $M_{\text{crit}} = 0.013$. For cooling turbine blades, blowing ratios ranging from $F = 0.5$–2.0 and density ratios of $\rho_c/\rho_e \approx 1$ are typical, which leads to momentum ratios ranging from $M = 0.25$–4.00. Even for high density ratios of $\rho_c/\rho_e \approx 4$, the momentum ratio in this study is still an order of magnitude smaller than those typical for turbine blade cooling. Finally, the low momentum ratios and the lack of turbulent mixing in the boundary layer make the cooling effectiveness independent of the momentum ratio or the blowing geometry. This has been determined by numerical simulations and in experiments for the investigated flow conditions (Fig. 16). With respect to the numerical simulations, the slot width has been varied from $s = 0.25$ to 2.0 mm and the blowing angle from 30 to 90 deg. In the experiments, the slot widths, $s_1 = 0.5$ mm and $s_2 = 1.0$ mm, and blowing angles, $\Omega_1 = 45$ and 90 deg, have been considered. All other parameters have been kept constant. For a constant cooling gas mass flow, that is, $Fs = \text{constant}$, the same cooling effectiveness is achieved independent of the slot geometry or the blowing ratio, that is, the cooling effectiveness is independent of the momentum ratio. In addition to varying the slot width s in the streamwise direction, the slot length t in spanwise direction has also been varied experimentally to ensure the two-dimensionality of the flow problem. For $t \geq 90$ mm, the vortices at the edge of the blowing opening no longer have a measurable effect on the cooling effectiveness. Thus, all presented results achieved for a slot width of $t = 120$ mm can be regarded as two dimensional, at least for the measuring section at the midspan.

Besides the slot geometry, the momentum ratio can be varied by altering the temperature ratio between the cooling gas and the mainstream. For numerical simulations, the cooling gas temperature has been varied from $T_c = 200$ to 400 K for the fixed mainstream temperature and blowing ratio. According to Eq. (24), this variation is equal to a momentum ratio variation of $\pm 33\%$ with respect to a cooling gas temperature of 300 K. In agreement with the earlier results, the change in the momentum ratio has no influence on the cooling effectiveness; all considered cooling gas temperatures result in the same cooling effectiveness. Because of higher cooling gas temperatures, the absolute cooling effect decreases, that is, the adiabatic wall temperature, $T_{\text{aw},c}$, increases and the term $T_r - T_{\text{aw},c}$ in

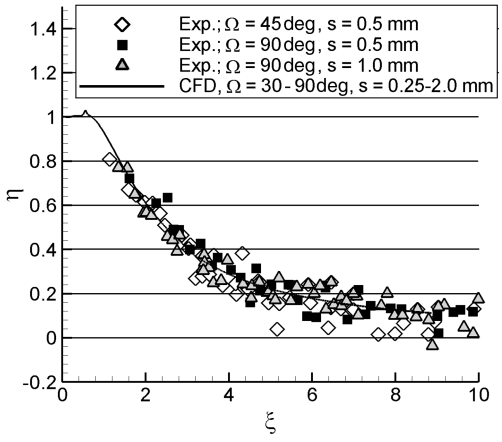

Fig. 16 Influence of slot geometry, condition Ib.

Eq. (3) decreases. In contrast, the cooling capacity described by the temperature difference $T_r - T_{c,0}$ also decreases because of the increase in the cooling gas temperature. Thus, the ratio of both temperature differences remains constant. Consequently, the cooling effectiveness stays constant.

E. Influence of the Thermal Wall Conditions

Unlike in the performed experiments, the surface of a reentry body is heated up to high temperatures during reentry. The maximum theoretically possible wall temperature is the adiabatic wall temperature. As detailed in the general description in Sec. II, the wall temperatures for the adiabatic wall case can be correlated to the wall heat fluxes for cold isothermal walls provided that the heat transfer coefficients for the cases with and without cooling are equal. According to Eqs. (3), (5), and (6), the ratio of the heat transfer coefficients is given by the following expression valid for the considered case $T_w = T_{0,c}$ and $T_r = T_{\mathrm{aw,nc}}$:

$$\frac{\lambda_{\mathrm{nc}}}{\lambda_c} = \frac{\dot{q}_{\mathrm{nc}}}{\dot{q}_c} \cdot \frac{T_{\mathrm{aw},c} - T_w}{T_{\mathrm{aw,nc}} - T_w} = \frac{1 - \eta_{\mathrm{Eq.\ (3)}}}{1 - \eta_{\mathrm{Eq.\ (6)}}} \tag{25}$$

To determine the cooling effectiveness according to Eqs. (3) and (6), the flow along a flat plate has been simulated numerically for isothermal and adiabatic wall conditions. In Fig. 17, the cooling effectiveness determined by Eq. (3) for the adiabatic case is compared with the effectiveness determined by Eq. (6) for the case of an isothermal wall of $T_w = 300$ K. Downstream from the blowing opening, no significant deviation occurs for either case. Thus, for the conditions presented in this work, the cooling effectiveness determined from the heat flux data for a cold wall case and the cooling effectiveness determined for adiabatic wall conditions are equal. Finally, according to Eq. (25), the heat transfer coefficients for the cases with and without cooling are equal. Moreover, both definitions for the cooling effectiveness [Eqs. (3) and (6)] can be used for considering a stationary flight case. Within the considered range of nearly perfect gas behavior, neither the total temperature nor the recovery temperature do not affect this result.

F. Influence of Freestream Conditions

According to the definition of the correlation factor given in Eq. (18), the conditions at the boundary-layer edge influence the cooling effectiveness via the Reynolds and Mach numbers and the static temperature. In this subsection, these parameters have been varied to confirm this relation.

The Reynolds number of the freestream at the slot position has been varied, on the one hand, by changing the distance, x_s, of the blowing opening from the leading edge. On the other hand, the unit Reynolds number has been slightly changed. Analogous to a laminar compression corner flow, the size of the separation bubble in front of the blowing opening increases with an increasing Reynolds number [28]. This effect becomes obvious in Fig. 18 by the increasing cooling effectiveness in front of the cooling slot with increasing Reynolds numbers, which is not directly caused by the cooling gas but by reduced wall heat fluxes within the separation bubble. The cooling effectiveness downstream of the slot shows a weaker decrease for larger running lengths and constant unit Reynolds number, because the thicker boundary layer results in smaller gradients within the boundary layer. In this case, the lower velocity and lower temperature act at the outer edge of the cooling gas layer, leading to lower gradients across the cooling layer. Ultimately, this results in a reduced heating of the cooling gas, which leads to an increasing cooling effectiveness with increasing running length. For a constant running length and higher unit Reynolds number, the oncoming boundary layer is thinner; consequently, the gradients within the boundary layer are steeper, which should actually cause a greater heating of the cooling gas. However, this effect of greater heating of the cooling gas is counterbalanced by the fact that, according to Eqs. (12) and (13), the mass flow of the hot gas entering the mixing layer with respect to the cooling gas mass flow is less than for a lower unit Reynolds number in the case of a constant blowing ratio. To summarize, the cooling effectiveness increases with increasing unit Reynolds number.

For a constant Reynolds number and blowing ratio, the influence of the Mach number has been investigated in the range of $Ma = 1.6$–4.0. The numerical simulations are performed for adiabatic wall conditions. Unlike the previously cited investigations, the variation of the Mach number results in coupled effects on the relevant parameters. With an increasing Mach number, the recovery temperature of the main flow increases for a constant, static freestream temperature or the static temperature decreases for a constant recovery temperature. Furthermore, the thickness of the oncoming boundary layer increases with increasing Mach number. Even for constant Mach numbers, that is, a constant temperature ratio but different static and total temperature levels, the boundary-layer profile of the oncoming boundary layer changes with the temperature level due to different viscosity and density levels in the boundary layer. These temperature viscosity effects are typical for compressible flows. The influence of these temperature viscosity effects as well as the compressibility effects associated with them are described by the square root of the Chapman–Rubesin factor in laminar flows without cooling gas injection [21].

The blowing parameters (F, $\dot{m}_c$, and T_c) and the Reynolds number of the freestream have been kept constant for the following discussion. As shown in Fig. 19, a lower cooling effectiveness is achieved for a lower Mach number. The cooling effectiveness also shows a slight difference (Fig. 19) in the case of an equal Mach number and different static and recovery temperatures, respectively. Comparing the lower Mach number case with the higher Mach number case under the condition of an equal recovery temperature, the same tendency is observed for the low Mach number compared with the higher Mach number with the equal static temperature.

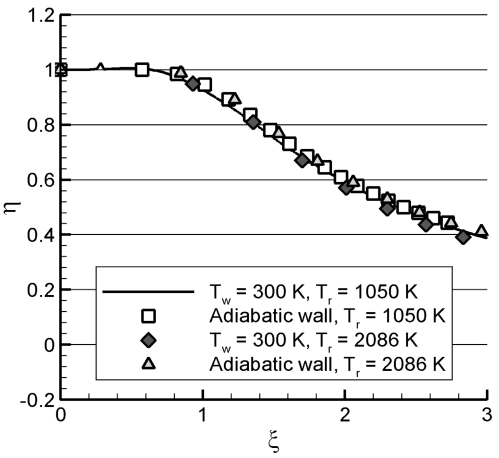

Fig. 17 Comparison of the adiabatic and isothermal wall conditions, $Ma = 2.6$, $Re = 4.3 \times 10^6$ m^{-1}, Fs = constant, CFD.

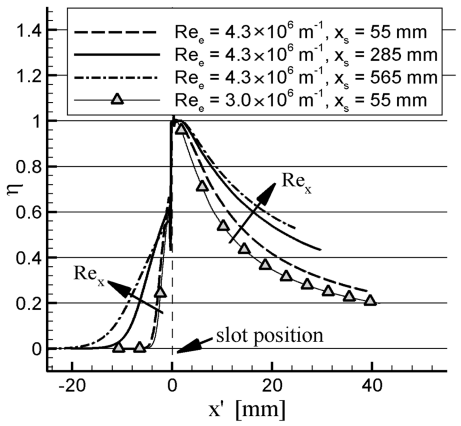

Fig. 18 Variation of the Reynolds number, $F = 0.065$, $s = 0.5$ mm, condition Ia, CFD.

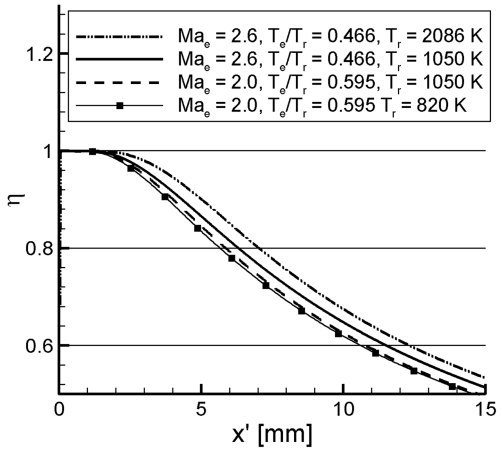

Fig. 19 Influence of the Mach number and temperature viscosity effects on the cooling effectiveness, CFD.

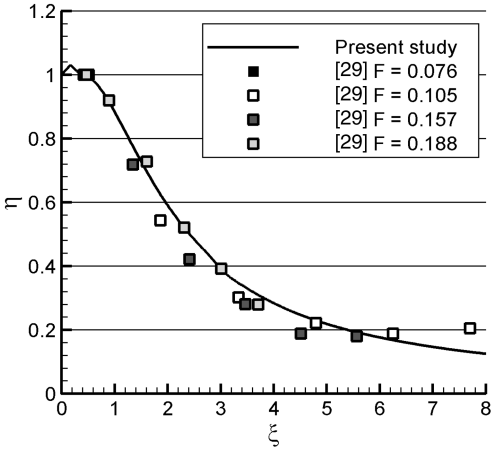

Fig. 21 Comparison with data from literature.

In Sec. III, it has been assumed that one of the main parameters influencing the cooling effectiveness is the mass flow of the mainstream entering the mixing layer, which is estimated by the mass flow of a regular boundary layer starting from the injection slot. Thus, this mass flow also depends on temperature viscosity effects just like a boundary layer without cooling gas injection. These temperature viscosity effects are described by the square root of the Chapman–Rubesin factor. With an increasing Mach number and an increasing freestream static temperature, the Chapman–Rubesin factor decreases, whereby the Mach number influence is stronger within the investigated range of flow conditions. Because of this, the cooling effectiveness increases with an increasing Mach number.

In Fig. 20, different results for different freestream conditions are plotted vs the correlation factor given in Eq. (18). In agreement with the experiments in which the flow conditions have been varied by changing the angle of attack of the flat plate, the numerical simulations show that the correlation factor captures all effects of changing flow conditions.

G. Comparison with Data from Literature

So far, the correlation factor developed in Sec. III has been validated with our own numerical simulations and experiments. In the following subsection, the presented results will be confirmed by comparing them with the data from literature. In [29], film cooling for laminar flow conditions and tangential slot injection was experimentally investigated for a Mach number of $Ma_e = 10$, a unit Reynolds number of $Re_e = 6 \times 10^6$ m^{-1}, a stagnation temperature of $T_0 = 1290$ K, and a distance of the slot to the leading edge of $x_s = 33$ mm. Furthermore, a theoretical approach was presented correlating the data for $\eta > 0.5$. For $\eta < 0.5$, the data

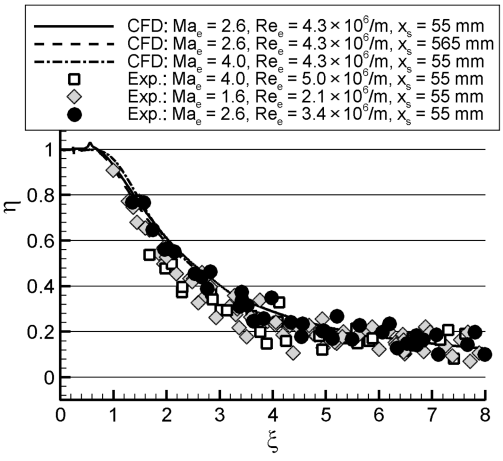

Fig. 20 Effect of varying freestream conditions.

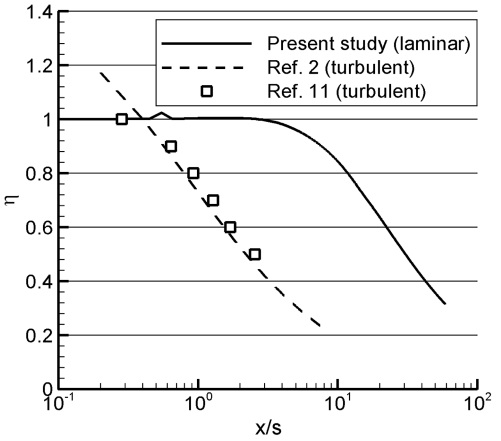

Fig. 22 Comparison of laminar and turbulent film cooling, condition Ia, $F = 0.065$, $s = 0.5$ mm.

differ from the correlation function, whereby this difference increases with decreasing cooling effectiveness. The considered blowing ratios range from $F = 0.05$ to 0.40 for slot heights between 0.8 and 1.6 mm. Figure 21 shows the results from [29] correlated with Eq. (18) in comparison with the data acquired in present study. Obviously, a good agreement between the data from [29] and the present study is achieved even for $\eta < 0.5$. Unlike the present study, no boundary-layer transition has been reported in [29], even for significantly higher blowing ratios, which is probably caused by the absence of a blowing velocity component perpendicular to the wall.

The comparison of results for laminar and turbulent flow conditions impressively shows the difference between these two types of flow (Fig. 22). In turbulent flow, the cooling effectiveness decreases much faster with increasing distance from the blowing opening than it does for a laminar boundary layer due to the turbulent mixing between the cooling gas and the main flow. For the same blowing and freestream conditions, the attainable cooling length is about an order of magnitude larger for the laminar case than for the turbulent case. To compare the data for the laminar and turbulent cases, that is, to relate them to the same Mach and Reynolds numbers, it has been assumed that the correlations given in [2,11] are also valid for the flow conditions considered in this paper.

VII. Conclusions

An enormous database of theoretical, experimental, and numerical data exists for film cooling in turbulent flow. However, very little data can be found in the literature for laminar flow conditions. The present study fundamentally investigates film cooling on a flat plate with a slot injection in laminar supersonic flows. In contrast to a

turbulent boundary layer, no turbulent mixing exists in the laminar case, and so the interaction between the main flow and the cooling gas behaves differently. In a turbulent flow, the mixing between the main flow and the cooling gas strongly depends on the blowing momentum perpendicular to the wall. This results in a decreasing cooling effectiveness with a higher blowing momentum perpendicular to the wall. Because of the lack of turbulent mixing in laminar conditions, the cooling effectiveness does not depend on the blowing momentum perpendicular to the wall, provided that the laminar boundary layer is not significantly disturbed. Moreover, in our study, the considered blowing momentum ratio between the cooling gas and the mainstream is about an order of magnitude lower than that typical for cooling turbine blades. Consequently, our experimental and numerical investigations show no influence of the blowing parameters, that is, the blowing ratio ($F = 0$–0.15), the slot width ($s = 0.25$–2.00 mm), the blowing angle ($\Omega = 30$–90 deg), and the cooling gas temperature ($T_c = 200$–400 K), on the cooling effectiveness, provided that the absolute cooling gas mass flow with respect to the specific mass flow in the main stream (Fs) is constant. Furthermore, as expected for a given cooling gas mass flow, the attainable cooling effect is significantly higher for a laminar flow than for a turbulent flow. For the laminar case, the cooling is limited by a critical blowing ratio for which boundary-layer transition occurs downstream from the injection position due to high blowing ratios. In this case, the heat loads to the wall rapidly increase and the surface is heated up instead of being cooled down. In our study, a critical blowing ratio of $F_{\text{crit}} = 0.144$ has been found for a slot width of 0.5 mm and for an injection perpendicular to the wall.

Varying the freestream conditions causes an increasing cooling effectiveness with increasing Mach and Reynolds numbers in the range of $Ma = 1.6$–4.0 and $Re = 0.17 \times 10^6$–2.4×10^6, which is evaluated with the distance between the leading edge of the model and the injection opening. This effect is covered by a theoretical model resulting from a simple heat sink approach that describes the thermal interaction between the cooling gas and the main flow. Finally, as the most important result, a correlation factor derived from this theoretical approach allows for the prediction of the cooling effectiveness under different flow conditions. This correlation factor has been validated by experiments and numerical simulations for the aforementioned flow conditions. In addition, the validity of the correlation factor has been proven by comparison with literature data. In summary, the presented fundamental research has shown that the film-cooling technique is highly effective under laminar flow conditions.

References

[1] Curry, D. M., "Space Shuttle Orbiter Thermal Protection System Design and Flight Experience," NASA TM-104773, 1993.

[2] Goldstein, R. J., "Film Cooling," *Advances in Heat Transfer*, edited by T. F. Irvine, and J. P. Hartnett, Vol. 7, Academic Press, New York, 1971, pp. 321–379.

[3] Taslim, M. E., Spring, S. D., and Mehlmann, B. P., "Experimental Investigation of Film Cooling Effectiveness for Slots of Various Exit Geometries," *Journal of Thermophysics and Heat Transfer*, Vol. 6, No. 2, 1992, pp. 302–307. doi:10.2514/3.359

[4] Fitt, A. D., Ockendon, J. R., and Jones, T. V., "Aerodynamics of Slot-Film Cooling: Theory and Experiment," *Journal of Fluid Mechanics*, Vol. 160, 1985, pp. 15–27. doi:10.1017/S0022112085003366

[5] Fitt, A. D., and Wilmot, P., "Slot Film Cooling—the Effect of Separation Angle," *Acta Mechanica*, Vol. 103, Nos. 1–4, March 1994, pp. 79–88. doi:10.1007/BF01180219

[6] Jung, K. H., "Multi-Row Film Cooling on Curved Surfaces (Mehrreihige Filmkühlung an Gekrümmten Oberflächen)," Ph.D. Thesis, Technical University of Darmstadt , Darmstadt, Germany, 2001.

[7] Thole, M., Gritsch, M., Schulz, A., and Wittig, S., "Flow Field Measurements for Film-Cooling Holes with Expanded Exits," American Society of Mechanical Engineers 96-GT-174, 1996.

[8] Thole, M., Gritsch, M., Schulz, and, A., Wittig, S., "Transonic Film-Cooling Investigations: Effects of Hole Shapes and Orientations," American Society of Mechanical Engineers 96-GT-222, 1996.

[9] Jubran, B. A., Al-Hamadi, A. K., and Theodoridis, G., "Film Cooling and Heat Transfer with Air Injection through Two Rows of Compound Angle Holes," *Heat and Mass Transfer 33*, Springer–Verlag, 1997, pp. 93–100.

[10] Baldauf, S., Schulz, A., and Wittig, S., "High Resolution Measurement of Local Heat Transfer Coefficients from Discrete Hole Film Cooling," *Journal of Turbomachinery*, Vol. 123, No. 4, Oct. 2001, pp. 749–757. doi:10.1115/1.1387245

[11] Holden, M. S., "Experimental Studies of Shock-Wave/Wall-Jet Interaction in Hypersonic Flow," NASA CR-195844, 1994.

[12] Juhany, K. A., and Hunt, M. L., "Flow Field Measurements in Supersonic Film Cooling Including the Effect of Shock-Wave Interaction," *AIAA Journal*, Vol. 32, No. 3, 1994, pp. 578–585. doi:10.2514/3.12024

[13] Juhnay, K. A., Hunt, M. L., and Sivo, J. M., "Influence of Injection Mach Number and Temperature on Supersonic Film Cooling," *Journal of Thermophysics and Heat Transfer*, Vol. 8, No. 1, 1994, pp. 59–65. doi:10.2514/3.501

[14] Aupoix, B., Mignosi, A., Viala, S., Bouvier, F., and Gaillard, R., "Experimental and Numerical Study of Supersonic Film Cooling," *AIAA Journal*, Vol. 36, No. 6, 1998, pp. 915–923.

[15] Gollnick, A. F., Jr., "Thermal Effects on a Transpiration Cooled Hemisphere," *Journal of the Aerospace Sciences*, Vol. 29, Aug. 1962, pp. 583–595.

[16] Fox, H., and Libby, P. A., "Helium Injection into the Boundary Layer at an Axisymmetric Stagnation Point," *Journal of the Aerospace Sciences*, Vol. 29, Aug. 1962, pp. 921–934.

[17] Lezuo, M. K., "Heat Transport in a H_2-Transpirative-Cooled Combustion Chamber (Wärmetransport in H_2-Transpirativ Gekühlter Brennkammer)," Ph.D. Thesis, DRheinisch Westfälischen Technischen Hochschule Aachen University, Aachen, Germany, 1998.

[18] Greuel, D., Serberst, E., and Haidn, O. J., "Use of Porous Fibre Ceramics for Effusion Cooling in the Nozzle of a Rocket Combustion Chamber (Einsatz von Porösen Faserkeramiken für Effusionskühlung im Düsenbereich von Raketenbrennkammern)," Deutsche Gesellschaft für Luft-und Raumfarht Paper JT2001-118, Hamburg, Germany, 2001.

[19] Anderson, J. D., *Hypersonic and High Temperature Gas Dynamics*, 2nd ed., AIAA, Reston, VA, 2000, Chaps. 6, 16, ISBN 1-56347-459-X.

[20] Van Driest, E. R., "Investigation of a Laminar Boundary Layer in Compressible Fluid Using the Crocco Method," NACA TN2597, 1952.

[21] Simeonides, G., "Generalized Reference Enthalpy Formulations and Simulation of Viscous Effects in Hypersonic Flow," *Shock Waves*, Vol. 8, No. 3, June 1998, pp. 161–172. doi:10.1007/s001930050109

[22] Schultz, D. L., and Jones, T. V., "Heat Transfer Measurements in Short Duration Hypersonic Facilities," NATO AGARDograph 165, 1973.

[23] Grönig, H., and Olivier, H., "Experimental Hypersonic Flow Research in Europe," *JSME International Journal. Series B, Fluids and Thermal Engineering*, Vol. 41, No. 2, 1998, pp. 397–407.

[24] Olivier, H., Jiang, Z., Yu, H. R., and Lu, F., "Detonation-Driven Shock Tubes and Tunnels," *Advanced Hypersonic Test Facilities*, edited by F. Lu, and D. Marren, Vol. 198, Progress in Astronautics and Aeronautics, AIAA, Reston, VA, 2002, pp. 135–203.

[25] Heufer, K. A., and Olivier, H., "Film Cooling for Hypersonic Flow Conditions," *Proceedings of the 5th European Workshop on Thermal Protection Systems and Hot Structures*, SP-631, ESA, Paris, 2006.

[26] Toro, E. F., *Riemann Solvers and Numerical Methods for Fluid Dynamics*, Springer–Verlag, Berlin/New York/Heidelberg, 1997, ISBN: 3540616764.

[27] Gruber, M. R., Nejad, A. S., Chen, T. H., and Dutton, J. C., "Mixing and Penetration Studies of Sonic Jets in a Mach 2 Freestream," *Journal of Propulsion and Power*, Vol. 11, No. 2, 1995, pp. 315–323. doi:10.2514/3.51427

[28] Lewis, J. E., Kubota, T., and Lees, L., "Experimental Investigation of Supersonic Laminar, Two-Dimensional Boundary-Layer Separation in a Compression Corner with and Without Cooling," *AIAA Journal*, Vol. 6, No. 1, 1968, pp. 7–14. doi:10.2514/3.4434

[29] Richards, B. E., and Stollery, J. L., "Laminar Film Cooling Experiments in Hypersonic Flow," *Journal of Aircraft*, Vol. 16, No. 3, 1979, pp. 177–181. doi:10.2514/3.58502

N. Chokani
Associate Editor